The 6th International Supercritical $CO_2$ Power Cycles Symposium
March 27 - 29, 2018, Pittsburgh, Pennsylvania

# Numerical Investigation of Transonic Supercritical CO2 Flows with Nonequilibrium Condensation in a Laval Nozzle

**Hironori MIYAZAWA**
Ph.D. Student
Tohoku University
Sendai, Japan
miyazawa@caero.mech.tohoku.ac.jp

**Takashi FURUSAWA**
Assistant Professor
Tohoku University
Sendai, Japan
furusawa@caero.mech.tohoku.ac.jp

**Satoru YAMAMOTO**
Professor
Tohoku University
Sendai, Japan
yamamoto@caero.mech.tohoku.ac.jp

## ABSTRACT

In this paper, we numerically investigate the nonequilibrium condensation of supercritical $CO_2$ flows in an axisymmetric Laval nozzle. Our numerical method was originally developed for moist-air flows over an airfoil and wet-steam flows in steam turbines. This method was coupled with the thermophysical database, REFPROP, and applied to the simulation of the transonic supercritical $CO_2$ flows with nonequilibrium condensation. In the results, nonequilibrium condensation started near the throat, and the pressure and temperature were increased at the diverging area by the release of the latent heat. The position of the maximum nucleation rate of $CO_2$ liquid particles was moved by changing the inlet temperature, resulting in the pressure difference at the diverging area. The results indicate that the condensation certainly affects the performance of the Laval nozzle.

## INTRODUCTION

Supercritical $CO_2$ Brayton cycles have been studied for developing a compact and efficient power generation with solar power, fossil fuel, geothermal energy, exhaust heat, and other many heat sources. Since a radial compressor working along the cycle is considered to compress the supercritical $CO_2$ near the critical point, the accurate prediction of the performance is a primary issue to design the compressors. Changing the impeller shape to decrease secondary vortices may be one of the standard approaches to improve the performance. Pressure and temperature in the compressor working in the supercritical state may conditionally decrease in the flow passage as crossing the saturated values. A strong supercooled condition may induce nonequilibrium condensation of $CO_2$ gas, forming $CO_2$ liquid particles in the flow passage. Therefore, the condensation of $CO_2$ is another issue to be predicted for designing the supercritical $CO_2$ compressor.

Recently, supercritical and high-pressure $CO_2$ flows with nonequilibrium condensation were numerically and experimentally investigated by some researchers. Rinaldi et al. [1] and Ameli et al. [2] numerically studied a supercritical $CO_2$ flow in a radial compressor and predicted the saturation condition in the flow path. Lettieri et al. [3] and Paxson et al. [4]

experimentally investigated supercritical and high pressure $CO_2$ flows with condensation in a Laval nozzle. Nonetheless, the fundamental investigation of supercritical $CO_2$ flows is still not sufficient for understanding condensate phenomena in supercritical conditions.

Our group has developed a numerical method for supercritical-fluid flows in which a preconditioning method [5] and the thermophysical database, PROPATH [6], was employed. The method was applied to several supercritical $CO_2$ problems [7][8]. We also developed another numerical method [9] to simulate transonic moist-air flows over an airfoil and transonic wet-steam flows in a steam turbine with nonequilibrium condensation and applied the method to several flow problems [9][10]. The obtained results indicate that nonequilibrium condensation certainly affects the performance of the airfoil and the steam turbine. In this study, we coupled our numerical method [9] with the Reference Fluid Thermodynamic and Transport Properties Database (REFPROP) developed by National Institute for Standards and Technology (NIST) to simulate supercritical $CO_2$ flows with the accurate thermophysical properties. In this paper, we applied the method to supercritical $CO_2$ flows in a Laval nozzle to understand the basis of nonequilibrium condensation in transonic supercritical $CO_2$ flows. The flows while changing the inlet temperature are calculated and the results are compared with each other.

## NUMERICAL METHODS

### Fundamental equations

Two-dimensional compressible Navier-Stokes equations, which comprise of the conservation laws for total density, momentum, total energy, are solved with conservation equations for density of $CO_2$ liquid particles and the number density. These equations are coupled with SST turbulence model [11]. Flows are assumed as a homogeneous flow without any slippage between the gas phase and the liquid particles since the particles are sufficiently small. The set of equations is written as

$$\frac{\partial Q}{\partial t} + L(Q) \equiv \frac{\partial Q}{\partial t} + \frac{\partial E_i}{\partial \xi_i} + F_v + H + H_{axi} = 0 \quad (i = 1,2) , \tag{1}$$

where $Q$, $E_i$ ($i$ = 1, 2), $F_v$, $H$, and $H_{axi}$ are the vectors of unknown variables, the flux, the viscous term, the source term, and the axisymmetric term, respectively, and are defined by

$$Q = J\begin{bmatrix} \rho \\ \rho u_1 \\ \rho u_2 \\ e \\ \rho\beta \\ \rho n \\ \rho k \\ \rho\omega \end{bmatrix}, \quad E_i = J\begin{bmatrix} \rho U_i \\ \rho u_1 U_i + \dfrac{\partial \xi_i}{\partial x_1} p \\ \rho u_2 U_i + \dfrac{\partial \xi_i}{\partial x_2} p \\ (e+p)U_i \\ \rho\beta U_i \\ \rho n U_i \\ \rho k U_i \\ \rho\omega U_i \end{bmatrix}, \quad F_v = -J\frac{\partial \xi_i}{\partial x_j}\frac{\partial}{\partial \xi_i}\begin{bmatrix} 0 \\ \tau_{1j} \\ \tau_{2j} \\ \tau_{kj}u_k + (\kappa + \kappa^t)\dfrac{\partial T}{\partial x_j} \\ 0 \\ 0 \\ \sigma_{kj} \\ \sigma_{\omega j} \end{bmatrix},$$

$$H = -J\begin{bmatrix} 0 \\ 0 \\ 0 \\ 0 \\ \Gamma \\ I \\ S_k \\ S_\omega \end{bmatrix}, \quad H_{axi} = J\frac{u_2}{r}\begin{bmatrix} \rho \\ \rho u_1 \\ \rho u_2 \\ e+p \\ \rho\beta \\ \rho n \\ \rho k \\ \rho\omega \end{bmatrix}.$$

where $\sigma_{kj}$, $\sigma_{\omega j}$, $S_k$, and $S_\omega$ are the dissipation and the source terms of $k$ and $\omega$, respectively. $\tau_{ij}$ is the viscous stress tensor component as follows:

$$\tau_{ij} = (\mu + \mu_t)\left[\left(\frac{\partial u_i}{\partial x_j} + \frac{\partial u_j}{\partial x_i}\right) - \frac{2}{3}\delta_{ij}\frac{\partial u_k}{\partial x_k}\right] \quad (i, j = 1,2). \tag{2}$$

$\Gamma$ and $I$ in Eq. (1) are the nucleation rate and the growth rate of $CO_2$ liquid particles which are based on our previous studies [9][10]. In addition, a modified nucleation rate considering real gas effect proposed by our group was employed in this study [12].

The compact MUSCL TVD scheme [13] and the Roe scheme [14] are used for the space discretization of convection terms in Eq. (1). The viscosity term is calculated by the second-order central-difference scheme. The LU-SGS scheme [15] is employed for the time integration.

**Equation of state for real gas and thermophysical properties**

Because intermolecular forces should be considered for fluids at a high-pressure state, equation of state (EOS) for real gas is employed with the governing equation (Eq. (1)). Since generally the mean radius of condensed droplets in transonic two-phase nozzle flows is sufficiently small (less than 1μm), we assume a homogeneous flow in which the pressure and temperature of liquid particles are the same with those of gas phase. The density and internal

energy of gas phase are calculated from the total density:

$$\rho_g = \rho(1-\beta)\frac{\rho_l}{(\rho_l - \beta\rho)}, \tag{3}$$

$$\varepsilon_g = \frac{\varepsilon - \beta C v_l T}{1-\beta}. \tag{4}$$

The pressure and temperature are calculated by the polynomial equations defined in REFPROP as the function of the density (Eq. (3)) and the internal energy (Eq. (4)). Thermophysical properties of the supercooled $CO_2$ are also required to simulate $CO_2$ flows. However, REFPROP does not cover those under the supercooled condition. In this study, the pressure and temperature are determined by the linear extrapolation using values on the saturated vapor line, written as

$$p(\rho_g, \varepsilon_g) = p(\rho_g)_{sat} + \Delta p(\rho_g)_{sat}\left(\varepsilon(\rho_g)_{sat} - \varepsilon_g\right), \tag{5}$$

$$T(\rho_g, \varepsilon_g) = T(\rho_g)_{sat} + \Delta T(\rho_g)_{sat}\left(\varepsilon(\rho_g)_{sat} - \varepsilon_g\right). \tag{6}$$

where the subscript “sat” means the value near the saturated vapor line, and $\Delta p$ and $\Delta T$ are the gradients near the saturated vapor line.

Figures 1(a) and 1(b) show the pressure and temperature plotted on density-internal energy diagram for $CO_2$. Our numerical method calculates the pressure and the temperature from linearly interpolated density and internal energy in these look-up tables. Thermophysical properties such as isobaric specific heat, viscosity, and thermal conductivity are also calculated from REFPROP.

Figures 2(a) and 2(b) show the viscosity and the thermal conductivity plotted on pressure-temperature diagram for $CO_2$. The thermophysical properties under the supercooled gas condition are assumed constant at the saturated vapor line. Also those of $CO_2$ liquid particles are assumed constant at 3.5MPa and 230K. The density, isobaric specific heat, viscosity, and thermal conductivity are $\rho_l$ = 1135 kg/m$^3$, $Cp_l$ = 1971.7 J/kg·K, $\mu_l$ = 2.093E-004 Pa, and $\kappa_l$ = 0.1656 W/m·K, respectively.

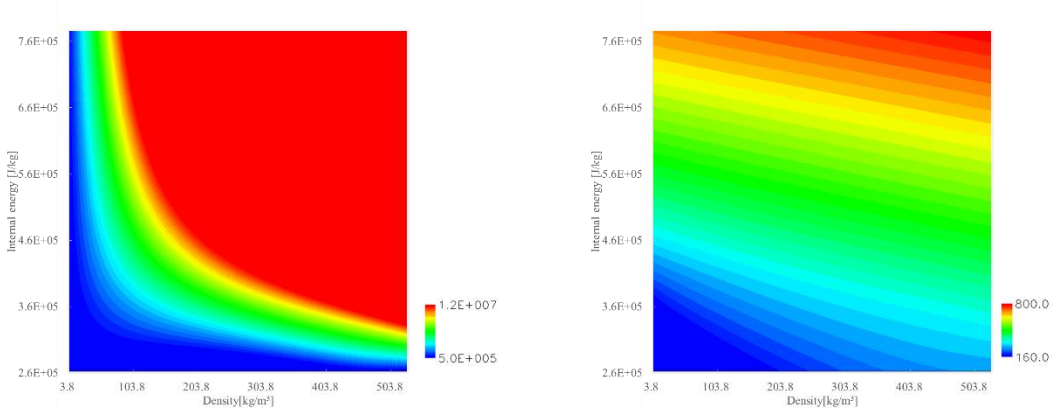


(a) Pressure (b) Temperature

Fig. 1 Density-Internal energy look-up tables calculated by REFPROP.

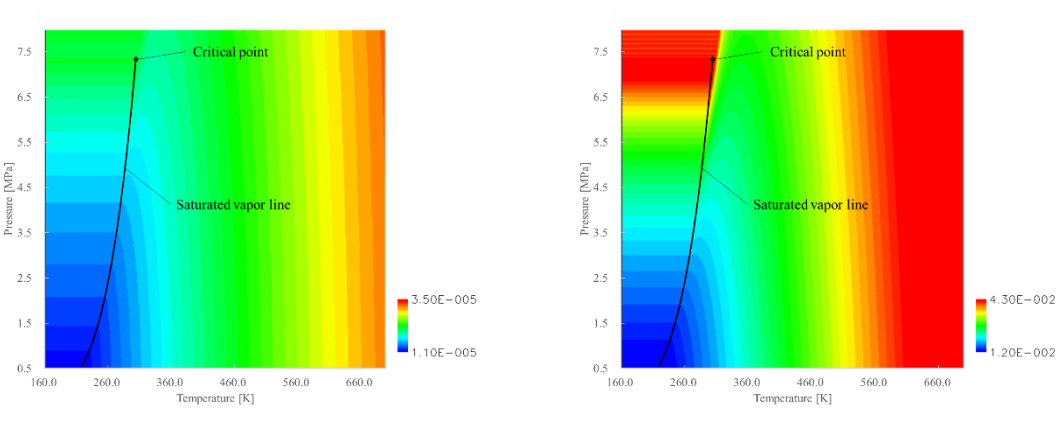


(a) Viscosity (b) Thermal conductivity

Fig. 2 Pressure-Temperature look-up tables for gas calculated by REFPROP.

## RESULTS AND DISCUSSION

In this study, transonic supercritical $CO_2$ flows with nonequilibrium condensation in a Laval nozzle are simulated. Figure 3 shows a schematic of the Laval nozzle experimentally investigated by Lettieri et al. [4] with the computational area. We assumed an axisymmetric flow. Figure 4 shows the computational grid. The nozzle geometry is generated based on the study by Yang [16].

Table 1 shows computational flow conditions. We consider three conditions, Case 1, Case 2, and Case 3. The inlet static pressure is fixed at 7.44 MPa in all cases. The inlet static temperatures are set to 315 K, 325 K, and 335 K for Case 1, Case 2, and Case 3, respectively. The inlet flow conditions are homogeneous, and the wall boundary is adiabatic condition.

Table 1 Computational flow conditions

| | $T_{in}$ [K] | $P_{in}$ [MPa] | Fluid | Nozzle diameter at the throat [mm] |
|---|---|---|---|---|
| Case 1 | 315 | 7.44 | | |
| Case 2 | 325 | 7.44 | $CO_2$ | 5.0 |
| Case 3 | 335 | 7.44 | | |

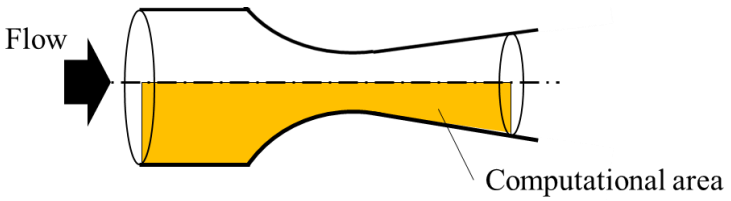


Fig. 3 Schematic of Laval nozzle with the computational area.

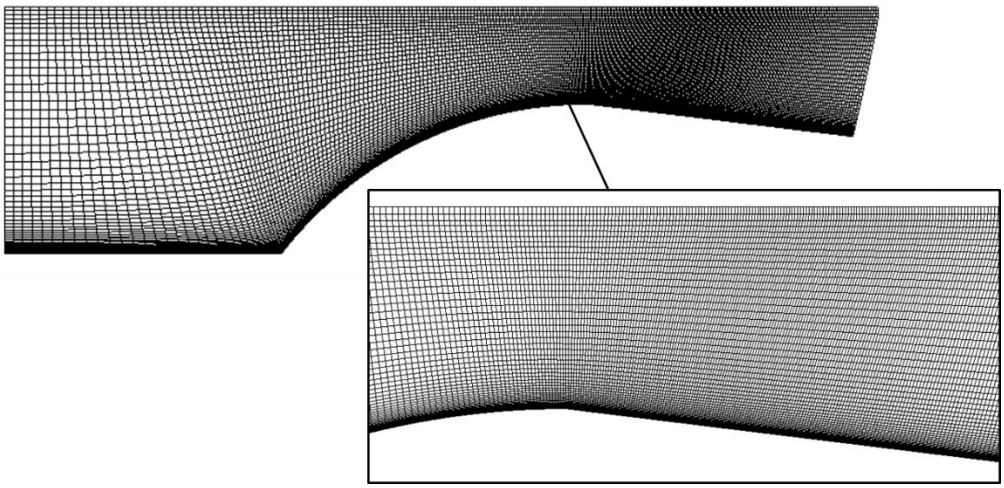

Fig. 4 Computational grid for axisymmetric Laval nozzle.

First, we simulated the flows of Case 2 with and without considering the condensation model to compare the results with and without the nonequilibrium condensation effect.

Figures 5(a), 5(b), and 5(c) show the static pressure, temperature, and Mach number contours without the condensation model, respectively. As shown in Figs. 5(a) and 5(b), the pressure and temperature decrease downward. The pressure and temperature reach to 0.65 MPa and 180 K at the outlet. A shock is generated near the nozzle throat and the flow becomes a supersonic speed at the diverging area where the Mach number finally reaches to 1.7 at the outlet as shown in Fig. 5(c).

Figures 6(a), 6(b), and 6(c) show the static pressure, temperature, and Mach number contours with the condensation model, respectively. In addition, Fig. 6(d) shows the condensate mass fraction. As shown in Fig. 6(d), condensation starts after the nozzle throat and the mass fraction increases up to 0.15 at the outlet. The values of pressure and temperature at the diverging area in Figs. 6(a) and 6(b) are higher than those in Figs. 5(a) and 5(b) assuming without the condensation model, while the Mach number at the diverging area is lower than that in Fig. 5(c). The weakened shock can also be observed near the throat with the condensation case as shown Fig. 6(c). Releasing the latent heat due to condensation increases the temperature, resulting in higher pressure and lower Mach number at the diverging area.

Figure 7 shows pressure-temperature plots for Case 2. The solid line and the dashed line represent the results with and without the condensation model, respectively. The plot with condensation model indicates that the pressure and temperature decrease rapidly, and becomes a supercooled condition. After the point around 3.15 MPa and 261 K at which nonequilibrium condensation starts, the pressure and temperature are increased by the release of latent heat. Such increments are not observed in the case without condensation model.

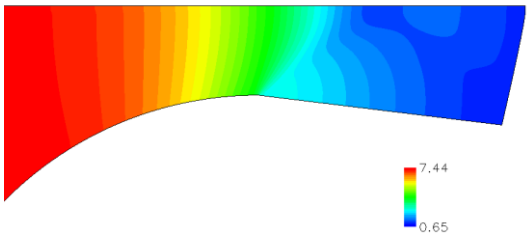


(a) Pressure (MPa)

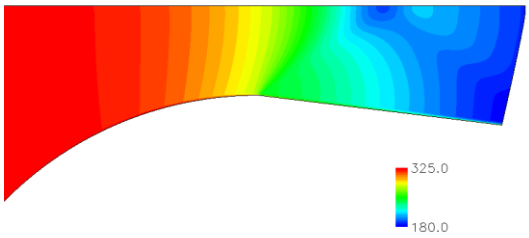


(b) Temperature (K)

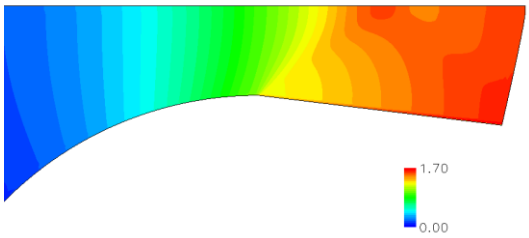


(c) Mach number (-)

Fig. 5 Results without condensation model for Case 2.

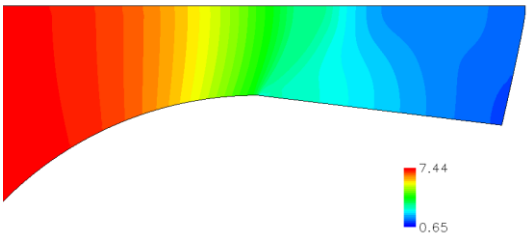


(a) Pressure (MPa)

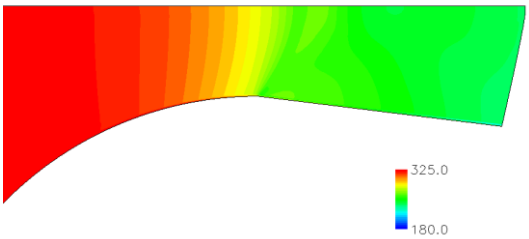


(b) Temperature (K)

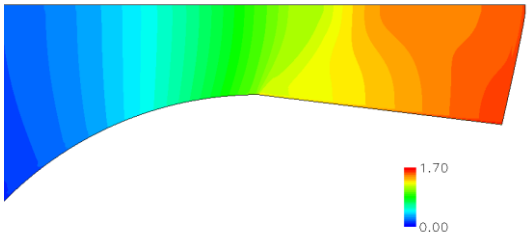


(c) Mach number (-)

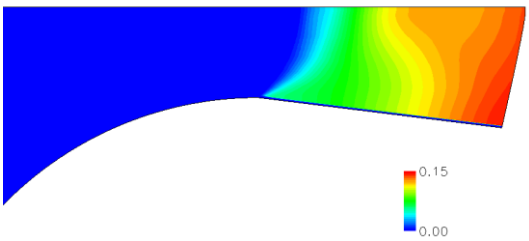


(d) Condensate mass fraction (-)

Fig. 6 Results with condensation model for Case 2.

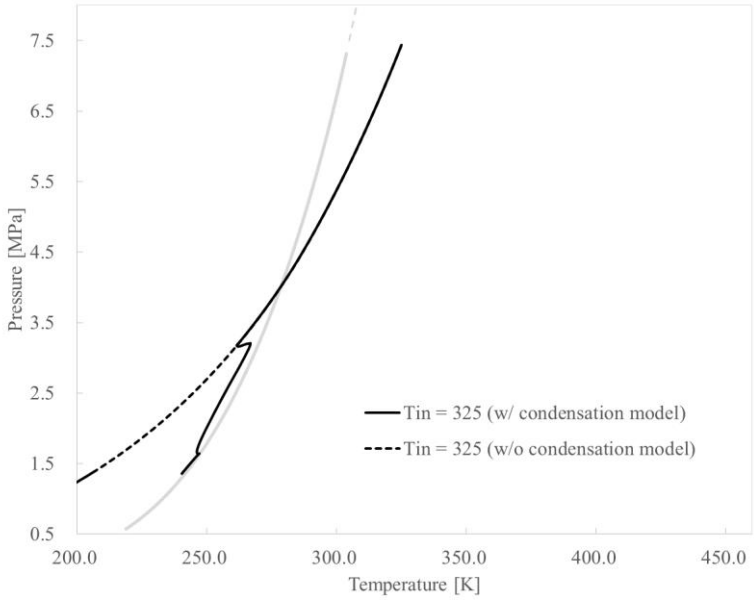


Fig. 7 Pressure-temperature plots with and without condensation model for Case 2.

Next, we focused on the inlet temperature affecting the $CO_2$ condensation.

Figures 8(a), 8(b), and 8(c) show the condensate mass fraction and nucleation rate contours for Case 1, Case 2, and Case 3, respectively. As shown in Fig. 8(a) and Fig. 8(b), nucleation occurs at the nozzle throat and nonequilibrium condensation starts after the nucleation. The onset of nucleation for Case 1 is slightly earlier than that of Case 2 and the condensate mass fraction at the diverging area is higher than that of Case 2, while the results for Case 3 in Fig. 8(c) represent a later onset of nucleation and lower condensate mass fraction than those of Case 2. These results indicate that the lower inlet temperature makes the onset of nucleation faster and the condensate mass generation higher.

Figure 9 plots the normalized pressure and nucleation rate distributions at the centerline of the nozzle for Case 1, Case 2, and Case 3. The dashed lines, solid lines, and dot lines correspond to Case 1, Case 2, and Case 3, respectively. The black and gray lines represent the pressure and nucleation rate, respectively. As shown in Fig. 8, the position of nucleation zone varies according to the change of inlet temperature. The maximum values of nucleation rate for Case 1 and Case 2 are almost the same, however, that for Case 3 is two orders lower than other cases. The pressure distribution of Case 2 coincides with that of Case 3 at the converging area, whereas that of Case 1 is relatively higher than other cases even without condensation. Since Case 1 is the closest condition to the critical point, the change of thermophysical properties may induce the change of the pressure distribution. The pressure starts to increase after the point at which the nucleation rate is the maximum value in all cases. Resultantly changing the inlet temperature was quite sensitive to the onset of nucleation and the condensation of $CO_2$.

Figure 10 shows the wall pressure distributions at the converging area compared with the

experimental results conducted by Lettieri et al. [3] [16]. The red dashed line, black solid line, and blue dashed line correspond to the numerical results for Case 1, Case 2, and Case 3, respectively. Although the pressure for Case 2 shows slightly higher value than that of other numerical cases, numerical results were fairly in agreement with the experimental results.

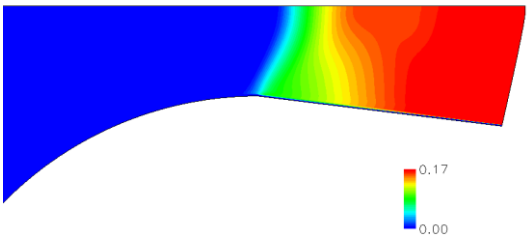


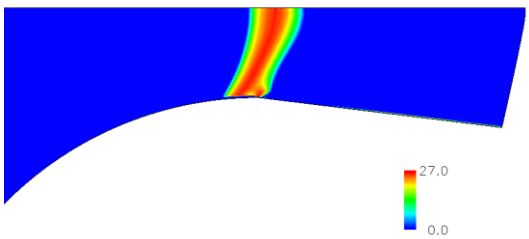


Condensate mass fraction Nucleation rate

(a) Case 1 ($T_{in}$ = 315K)

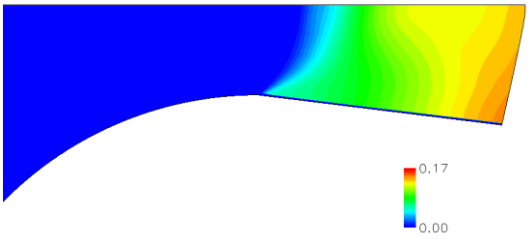


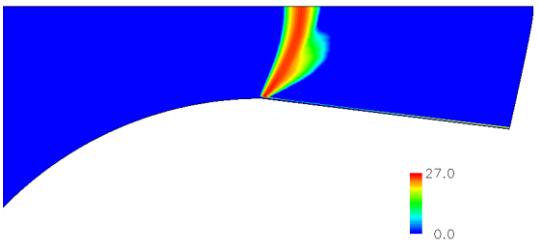


Condensate mass fraction Nucleation rate

(b) Case 2 ($T_{in}$ = 325K)

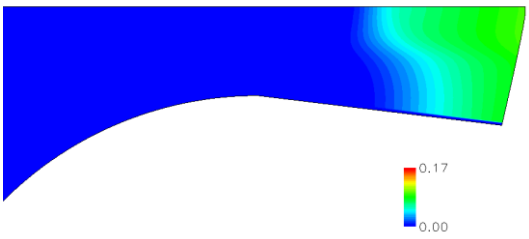


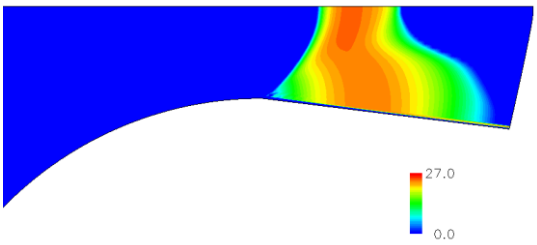


Condensate mass fraction Nucleation rate

(c) Case 3 ($T_{in}$ = 335K)

Fig. 8 Condensate mass fraction and nucleation rate (nucleation rate by common logarithmic value).

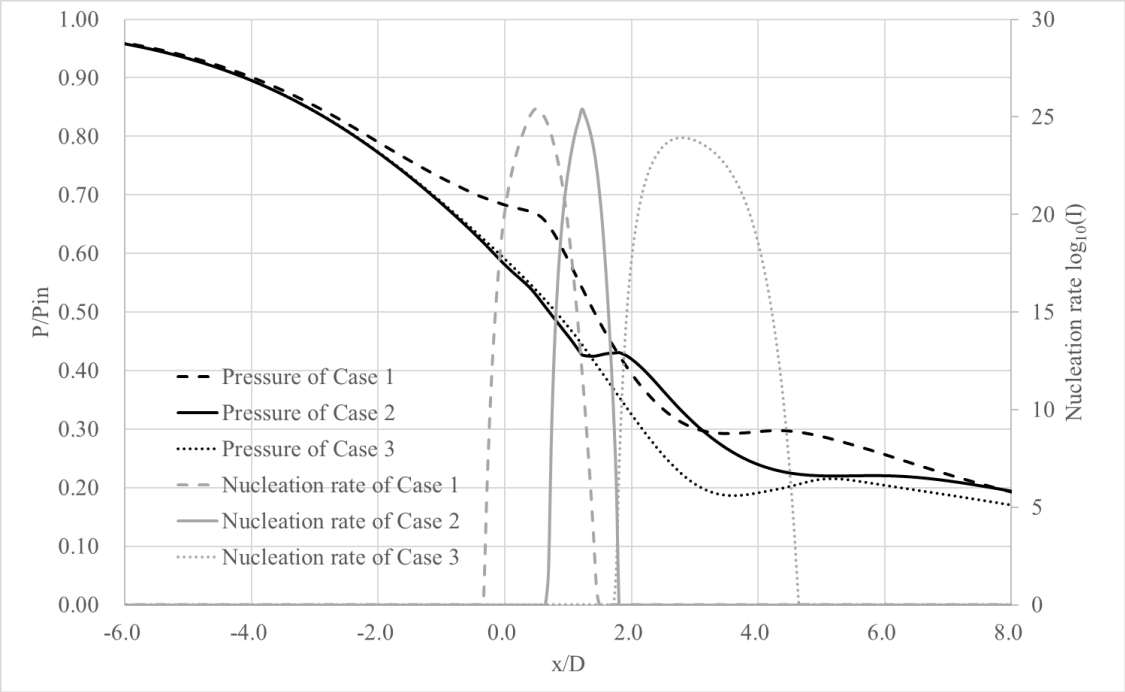


Fig. 9 Pressure and nucleation rate at the centerline of nozzle.

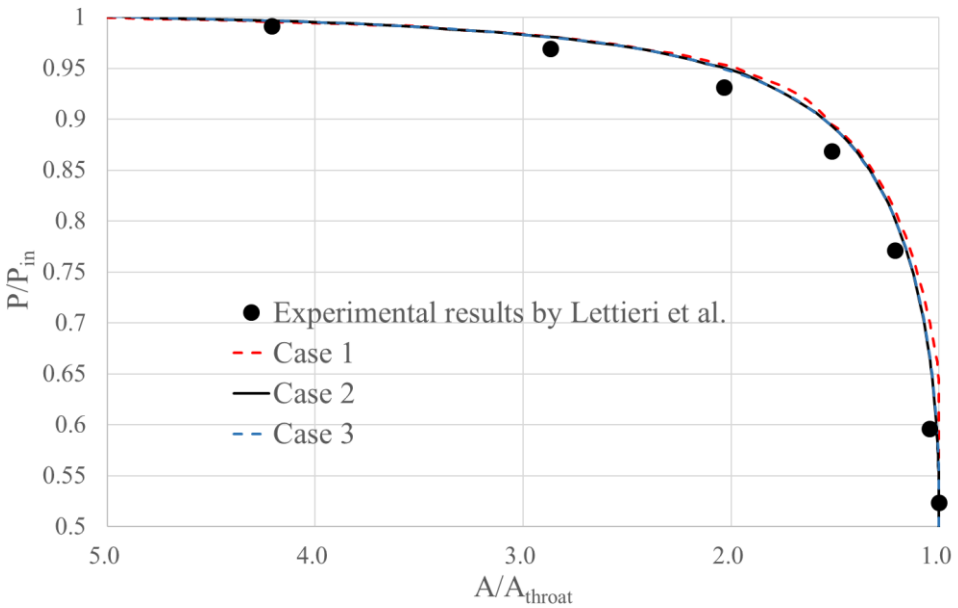


Fig. 10 Wall pressure distributions at the converging area.

## CONCLUSIONS

In this study, our numerical method coupled with REFPROP was applied to the simulation of a transonic supercritical $CO_2$ flow in a Laval nozzle. We investigated the nonequilibrium condensation in the supercritical $CO_2$ flow assuming the axisymmetric nozzle. Nonequilibrium condensation started near the throat, and the pressure and temperature were increased at the diverging area by the release of the latent heat. The position of the maximum

nucleation rate of $CO_2$ liquid particles was moved by changing the inlet temperature, resulting in the pressure difference at the diverging area. The results indicate that the condensation certainly affects the performance of the Laval nozzle. In addition, the pressure distribution at the converging area in the case assuming the inlet temperature closest to the critical point was slightly higher than that of other cases because of the effect of thermophysical values near the critical point.

## NOMENCLATURE

| | |
|---|---|
| $Cv$ | specific heat at constant volume |
| $e$ | total internal energy per unit volume |
| $I$ | homogeneous nucleation rate |
| $J$ | Jacobian of transformation |
| $k$ | turbulent kinetic energy |
| $n$ | number density of water droplets |
| $p$ | static pressure |
| $T$ | temperature |
| $t$ | physical time |
| $U_i$ | contravariant velocities ($i$ = 1,2) |
| $u_i$ | physical velocities ($i$ = 1,2) |
| $x_i$ | Cartesian coordinates ($i$ = 1,2) |
| $\beta$ | condensate mass fraction |
| $\delta_{ij}$ | the Kronecker's delta ($i$,$j$=1,2) |
| $\xi_i$ | general curvilinear coordinates ($i$ = 1,2) |
| $\rho$ | density |
| $\kappa$ | laminar thermal conductivity coefficient |
| $\kappa^t$ | turbulent thermal conductivity coefficient |
| $\mu$ | coefficient of molecular viscosity |
| $\mu_t$ | coefficient of turbulent viscosity |
| $\tau_{ij}$ | viscous stress tensors ($i$,$j$=1,2) |
| $\Gamma$ | mass generation rate |
| $\omega$ | turbulent kinetic energy dissipation ratio |

Subscripts

| | |
|---|---|
| $l$ | liquid phase |
| $g$ | gas phase |

## REFERENCES


[1] Rinaldi, E., Pecnik, R., and Colonna, P., Steady State CFD Investigation of a Radial Compressor Operating with Supercritical CO2, Proc. of ASME Turbo Expo 2013, 2013, GT2013-94580.

[2] Ameli, A., Afzalifar, A., Turunen-Saaresti, T. and Backman, J., Effects of Real Gas Model Accuracy and Operating Conditions on Supercritical CO2 Compressor Performance and Flow Field, Proc. ASME Turbo Expo 2017, 2017, GT2017- 63570.

[3] Lettieri, C., Yang, D. and Spakovszky, Z., An Investigation of Condensation Effects in Supercritical Carbon Dioxide Compressors, J. Eng. Gas Turbines Power 137-8, 2015, GTP-14-1592.

[4] Paxson, D., Lettieri, C., Spakovszky, Z., Bryanston-Cross, P. and Nakaniwa, A., Experimental Assessment of Thermodynamic Properties for Metastable CO2, Proc. 5th Int. Symp. Supercritical CO2 Power Cycles, 2016.

[5] Yamamoto, S., Preconditioning Method for Condensate Fluid and Solid Coupling Problems in General Curvilinear Coordinates, J. Comp. Physics, 207-1, 2005, 240-260.

[6] A Program Package for Thermophysical Properties of Fluids, Ver.12.1, PROPATH group.
[7] Yamamoto, S., Furusawa, T. and Matsuzawa, R., Numerical Simulation of Supercritical Carbon Dioxide Flows across Critical Point, Int. J. Heat and Mass Transfer, 54-4, 2011, 774-782.
[8] Yamamoto, S. and Furusawa, T., Thermophysical Flow Simulations of Rapid Expansion of Supercritical Solutions (RESS), J. Supercritical Fluids, 97, 2015, 192-201.
[9] Yamamoto, S., Computation of Practical Flow Problems with Release of Latent Heat, Energy, 30, 2005, 197–208.
[10] Miyazawa, H., Furusawa, T. and Yamamoto, S., Numerical Analysis of Condensation Effects on Final-Stage Rotor-Blade Rows in Low-Pressure Steam Turbine, J. Fluid Science and Technology, 12-2, 2017, 1-12.
[11] Menter, F. R., Two-Equation Eddy-Viscosity Turbulence Models for Engineering Applications, AIAA Journal, 32-8, 1994, 1598-1605.
[12] Furusawa, T. and Yamamoto, S., Mathematical Modeling and Computation of High-pressure Steam Condensation in a Transonic Flow, J. Fluid Science and Technology, 12-1, 2017, 1-11.
[13] Yamamoto, S. and Daiguji, H., Higher-Order-Accurate Upwind Schemes for Solving the Compressible Euler and Navier-Stokes Equations, Computers and Fluids, 22, 1993, 259-270.
[14] Roe, P.L., Approximate Riemann Solvers, Parameter Vectors and Difference Schemes, J. Comp. Phys., 43, 1981, 357-372.
[15] Yoon, S. and Jameson, A., Lower-upper Symmetric-Gauss-Seidel Method for the Euler and Navier-Stokes Equations, AIAA Journal, 26, 1988, 1025-1026.
[16] Yang, D., Experimental Assessment of the Internal Flow Behavior of Supercritical Carbon Dioxide, Master thesis, MIT, 2014.

## ACKNOWLEGEMENTS

This work was supported by KAKENHI, Grant-in-Aid for Scientific Research B, Grant-in-Aid for Young Scientists B and Grant-in-Aid for JSPS Research Fellow, promoted by the Japan Society for the Promotion of Science(JSPS)

## BIOGRAPHY

**Hironori Miyazawa**

Hironori Miyazawa is a Ph.D. student in Graduate School of Information Sciences at Tohoku University, Japan. His primary research area is the numerical simulation for the unsteady transonic flows with the nonequilibrium condensation in turbomachinery .

**Takashi Furusawa**

Dr. Takashi Furusawa is an Assistant professor in Graduate School of Information Sciences at Tohoku University, Japan. He received his Ph.D. from Tohoku University in 2012. His research interests are in the areas of numerical methods and numerical modeling for supercritical fluid flows.

**Satoru Yamamoto**

Prof. Satoru Yamamoto is a Professor in Graduate School of Information Sciences at Tohoku University, Japan. He received his Ph.D. from Tohoku University in 1989. His research field is Computational Fluid Dynamics (CFD) and Multiphysics CFD.